Available online at www.sciencedirect.com
SCIENCE DIRECT
ELSEVIER
Journal of the European Ceramic Society 26 (2006) 3017–3025
ECERS
www.elsevier.com/locate/jeurceramsoc

Structure and magnetism in the Zn–Mn–O system: A candidate for room temperature ferromagnetic semiconductor

J.F. Fernández [a,*], A.C. Caballero [a], M. Villegas [a], S.J. Khatib [b], M.A. Bañares [b], J.L.G. Fierro [b], J.L. Costa-Kramer [c], E. Lopez-Ponce [c], M.S. Martín-González [c], F. Briones [c], A. Quesada [d], M. García [d], A. Hernando [d]

[a] *Instituto de Cerámica y Vidrio, CSIC, C/Kelsen 5, 28049 Madrid, Spain*
[b] *Instituto de Catálisis y Petroleoquímica, CSIC, 28049 Madrid, Spain*
[c] *Instituto de Microelectrónica de Madrid, CSIC, C/Isaac Newton 8, 28760 Tres Cantos, Madrid, Spain*
[d] *Instituto de Magnetismo Aplicado "Salvador Velayos" RENFE-UCM-CSIC Las Rozas, P.O. Box 155, 28230 Madrid, Spain*

Available online 15 March 2006

Abstract

The reactivity of the Zn–Mn–O system, prepared by conventional ceramic routes using ZnO and MnO_2 as starting materials are described and correlated with the magnetic response. X-ray diffraction, X-ray photoelectron spectroscopy and Raman spectroscopy techniques have been used for the structural analysis. The ferromagnetic response is unambiguously determined to be due to the simultaneous presence of Mn^{+3} and Mn^{+4} ions at the Zn diffusion front into the manganese oxide grain. Thus, it is demonstrated that Mn does not incorporate into the ZnO lattice substitutionally, but it is the Zn that diffuses into the manganese oxide grains, acting as a retardant of the manganese reduction, $Mn^{+4} \rightarrow Mn^{+3}$. At the diffusion front, both ions coexist and their spins couple ferromagnetically through a double exchange mechanism. This mechanism explains the origin of the room temperature ferromagnetism recently discovered in Zn–Mn–O system as a promising material for spintronic devices.

Keywords: Powders-solid state reaction; X-ray methods; Magnetic properties; ZnO; Room temperature ferromagnetic semiconductors

1. Introduction

Carrier-induced ferromagnetism and dilute magnetic semiconductors (DMSs) are of much interest from the industrial viewpoint, because of their potential applications as new functional materials, opening a way to introduce the spin degree of freedom into semiconductor devices.[1] Current technologies require a continuous information exchange between semiconductors (controlling the logic) and the magnetic material that stores the information. High-speed semiconductor technologies are nowadays the base of a large amount of devices. The energy consumption and the high volatility of the information are disadvantages of these technologies. In magnetic materials the information storage relays on the magnetization orientation within the ferromagnetic material, being non-volatile devices. From the engineering point of view, materials combining both the semiconducting and the magnetic properties are of great interest. These ideal materials are key ingredients for the development of spintronic devices such as non-volatile, magnetic-semiconductor memories, spin-based field effect transistors, spin valve transistors, ultra fast optical switches or quantum computing devices. Tanaka[2] recently reported the huge potential of these new spintronic devices by using a new silicon-based spin metal-oxide-semiconductor field-effect transistor (spin MOSFET) consisting of a MOS gate and ferromagnetic contacts for the source and drain, from which an extremely large magneto-current ratio (more than 10,000%) can be obtained by flipping the magnetization from parallel to antiparallel. However, this device operates below room temperature because the Curie temperature, T_C, values of available ferromagnetic semiconductors were lower than 160 K.[2]

Since the prediction of the existence of ferromagnetic semiconductors at room temperature (RT FM), by Dietl et al.[3] there have been several experimental works reporting the appearance of ferromagnetism above 300 K. The systems based on ZnO are particularly interesting due to the fact that ZnO is a wide band semiconductor and is transparent in the visible part of the spectrum.

* Corresponding author. Tel.: +34 91 735 5840.
E-mail address: jfernandez@icv.csic.es (J.F. Fernández).

0955-2219/$ – see front matter © 2006 Elsevier Ltd. All rights reserved.
doi:10.1016/j.jeurceramsoc.2006.02.021

Sharma et al.[4] recently reported the first observation of room temperature ferromagnetism in Mn-doped ZnO pellets annealed at 500 °C, both bulk samples and thin films. The authors claimed that annealing process yields to the diffusion of Mn^{2+} into ZnO grains, giving rise to Mn-doped ZnO that shows carried induced ferromagnetism behaviour up to room temperature. Kundaliya et al.[5] suggested that the ferromagnetism originates in a metastable phase rather than by carrier-induced interaction between separated atoms in ZnO. They suggested the presence of a metastable phase, $Mn_{2-x}Zn_xO_{3-\delta}$, formed at low temperature by diffusion of Zn into the manganese oxide as the origin of ferromagnetism rather than by carried-induced interaction between separated atoms in ZnO. In a recent paper[6], RT FM was confirmed in samples prepared following the Sharma et al.[4] method. The compacts obtained from the low temperature treatment showed brittle characteristics of unreacted and poorly densified ceramic samples. Structural analysis points to non-homogeneous materials. Only a weak diffusion of Zn into MnO_2 grains is observed, whereas the presence of Mn into the ZnO matrix is never detected. More recently, García et al.[7] associated the ferromagnetism in Mn–Zn–O with the coexistence of Mn^{3+} and Mn^{4+} via a double-exchange mechanism. The presence of ZnO in the MnO_2 particles modifies the manganese reduction kinetics and favours the coexistence of both oxidation states. The ferromagnetism was associated with the interface formed at the Zn diffusion front into Mn oxide; this was corroborated by preparing thin films multilayers of ZnO and MnO_2 that exhibited saturation magnetization two orders of magnitude higher than bulk samples. This result was confirmed by the first principle calculation of Huang et al.[8] that suggests a size-dependent ferromagnetism coupling mechanism, due to a size-dependent transition from shallow acceptors to deep acceptors, and therefore rising to the FM stabilization to be dominated by double exchange via localized holes, rather than by free holes or by the Rudderman–Kittel–Kasuya–Yosaida (RKKY) mechanism.

Ferromagnetism in substituted zinc oxide has been the subject of numerous contributions[5] that in many cases show contradictory results and explanations, ranging from the absence of ferromagnetism to spin glass behaviour or low-temperature ferromagnetism. Venkatesan et al.[9] interpreted ferromagnetism in substituted ZnO in terms of a spin-split donor impurity-band model, which can account for ferromagnetism in insulating or conducting high-k oxides with concentrations of magnetic ions that lie far below the percolation threshold. Sluiter et al.[10], from first principles electronic structure calculations of transition metal substituted ZnO, developed a physical picture based on hybridization, super exchange, and double exchange that captures chemical trends. Thus, long-range interactions necessary for FM in diluted magnetic semiconductors can be mediated by defect-induced states as proved by co-doping ZnO:Co with Li^+. The decrease of saturation magnetization (M_s) observed for high temperature processed samples was attributed to the loss of Zn vacancies and Zn interstitials and their replacement with inert oxygen vacancies. According to Sharma et al.,[11] Mn–Zn–O samples processed at higher temperature than 500 °C lose their RT FM response because of segregation of antiferromagnetic Mn clusters. In these samples the possible presence of Mn_2O_3, $ZnMn_3O_7$ and $Zn_2Mn_3O_8$, implied an oxidation of the diluted Mn^{2+}. However, low-temperature chemical methods[12] failed to achieve magnetic order in Mn- and Co-doped ZnO and ensured that the dopants were located substitutionally. On the other hand, Kittilstved et al.[13] found enhancement of RT FM by chemical manipulation of Mn-doped ZnO nanocrystals with nitrogen that is related to higher concentration of Zn vacancies and interstitial sites.

The aim of this paper is to clarify the reactivity of the Zn–Mn–O system. It is clear that all properties depend on the processing method. In order to understand the nature of the phases involved in the appearance of RT FM behaviour, the ceramic processing route was chosen because it may provide accurate structural information. In addition, this system is of interest in the ceramic field because of several applications in which grain boundaries play an important role, as varistor ceramics,[14–16] are relevant; low-temperature reactions were not previously taken into account but in spite of the actual research may usefully be revisited. Other areas of interest of this system include catalysis applications and batteries.

2. Experimental procedure

Materials with different Mn concentrations were fabricated following the low-temperature procedure of Sharma et al.,[4,6] as follows: two particle-sized, high purity (>99.99%) ZnO powders with a d_{50} of 10.5 and 0.4 μm, respectively, and MnO_2 powder with d_{50} of 2.8 μm were used for sample preparation. In general, low particle size ZnO powders were used because of their higher reactivity, but for magnetic measurement both types of powders were used. In a first step, MnO_2 powders were 3 h attrition milled using 0.8 mm YTZP balls in water media. An ammonium salt of polyacrylic acid (0.1 wt.%) Duramax 3005 (Rhom and Haas, USA) was used as dispersant because of their low ash content. Compositions were homogenized by attrition milling and pre-reacted at 400 °C for 8 h. After that, pre-reacted powders were attrition milled again, axially pressed into disks at 100 MPa and exposed to a second thermal treatment at 500, 600, 700 and 900 °C for 12 h in air. Samples of different compositions based on $(ZnO)_{1-x}(MnO_2)_x$, with $x = 2.3$, 10.8, 51.7, 72.7 and 82 were processed. The first two compositions correspond to the $2MnO_2$–98ZnO and $10MnO_2$–90ZnO samples of Sharma et al.,[4] and will be thus named herein. The rest of the compositions are related to the Mn/Zn cation ratios of 1:1, 2:1 and 3:1, respectively. Note that the 2:1 ratio of Mn/Zn is the spinel composition, $ZnMn_2O_4$.

The density of samples was determined by the immersion Archimedes method, using mercury as the liquid medium. DTA-TG experiments were undertaken in a Nestzch STA 409 with a heating rate of 3 °C/min in air atmosphere. X-ray diffraction spectra, XRD, were obtained from powder samples and sintered pellets with a 1°/min 2Θ scan rate with a Siemens D5000 diffractometer, using Cu Kα radiation. Field emission scanning electron microscopy, FESEM, was carried out on freshly fractured samples. Magnetic properties were measured in a SQUID up to RT and in a high temperature VSM above RT.

Raman spectra were collected on a Renishaw Micro-Raman System 1000. The samples were excited with the 514 nm Ar line in an in situ treatment cell (Linkam TS-1500). For comparison purposes, reference materials without secondary crystalline phases were annealed or synthesized as follow: ZnO and MnO_2 annealed at 500 °C 12 h; Mn_2O_3 was obtained by annealing MnO_2 at 650 °C 8 h, and $ZnMn_2O_4$ was synthesized at 900 °C 12 h.

X-ray photoelectron spectra (XPS) were acquired with a VG ESCALAB 200R spectrometer provided with an Al Kα X-ray source (1486.6 eV). Kinetic energies of the photoelectrons of interest were measured using a hemispherical electron analyzer operating in the constant pass energy mode. The base pressure along the analysis was maintained below 5×10^{-9} mbar. Prior to analysis the samples were cleaned by ion-bombardment with an Ar^+ beam (2 kV) for 2 min. The XPS data were signal-averaged and taken in increments of 0.1 eV with dwell times of 30 ms. The binding energies were calibrated relative to the C1s peak from residual carbon contamination of the samples at 284.8 eV. High-resolution spectral envelopes were obtained by curve fitting synthetic peak components using the software package *XPS peak*. The raw data were used with no preliminary smoothing. Symmetric Gaussian–Lorentzian product functions were used to approximate line shapes of the fitting components.

Thin films were deposited on silicon substrates by a pulse laser deposition technique, PLD. Ceramic target were ablated using a Lambda Physik laser (model LPX 205i MC) operating ($\lambda = 193$ nm) with a pulse repetition rate of 10 Hz and pulse duration of 17 ns. The laser beam was focussed through a convex lens and a fused silica window into the vacuum chamber.

3. Results and discussion

Results from DTA-TG experiments on pure phases and mixtures of $2MnO_2$–$98ZnO$ and $10MnO_2$–$90ZnO$ samples are shown in Fig. 1. ZnO powders exhibited a slight mass increase up to 200 °C with adsorption of heat. This process is not a true endothermic reaction because it ranged across a wide range of temperatures and may be attributed to an artefact of the equipment, related both to the crucible location and the airflow in the furnace chamber. Further heating up to 425 °C yields to a small continuous mass loss. The increase of temperature could favour the release of oxygen from the ZnO crystal lattice and this process is the responsible for the white to yellow pale colour change of annealed ZnO powders. On the other hand, the partial vapour pressure of ZnO is relatively high at temperatures above 500 °C[17] and could also contribute to the mass loss.

A similar behaviour for the DTA base line up to 500 °C was found for MnO_2. A well defined exothermic peak centred at 190 °C, associated with a mass loss, is related to the dispersant used and is also present in the rest of samples. Starting at 525 °C the reduction process of MnO_2 to Mn_2O_3 is observed and at 925 °C a further reduction to Mn_3O_4 took place. The theoretical mass losses of these reactions[18] were in good agreement with experimental results from TG.

Mixtures of $2MnO_2$–$98ZnO$ and $10MnO_2$–$90ZnO$ showed different trends in the MnO_2 reduction process in addition to the ZnO evolution. Firstly, the MnO_2 reduction to Mn_2O_3 is uncompleted at 625 °C and requires higher temperature to be completed, pointing out the possible presence of the Mn_5O_8 phase[19] (equivalent to $MnO_{1.6}$). This phase, in a state of high purity, is a mixture of $Mn_2(II)Mn_3(IV)O_8$. Secondly, the endothermic peak

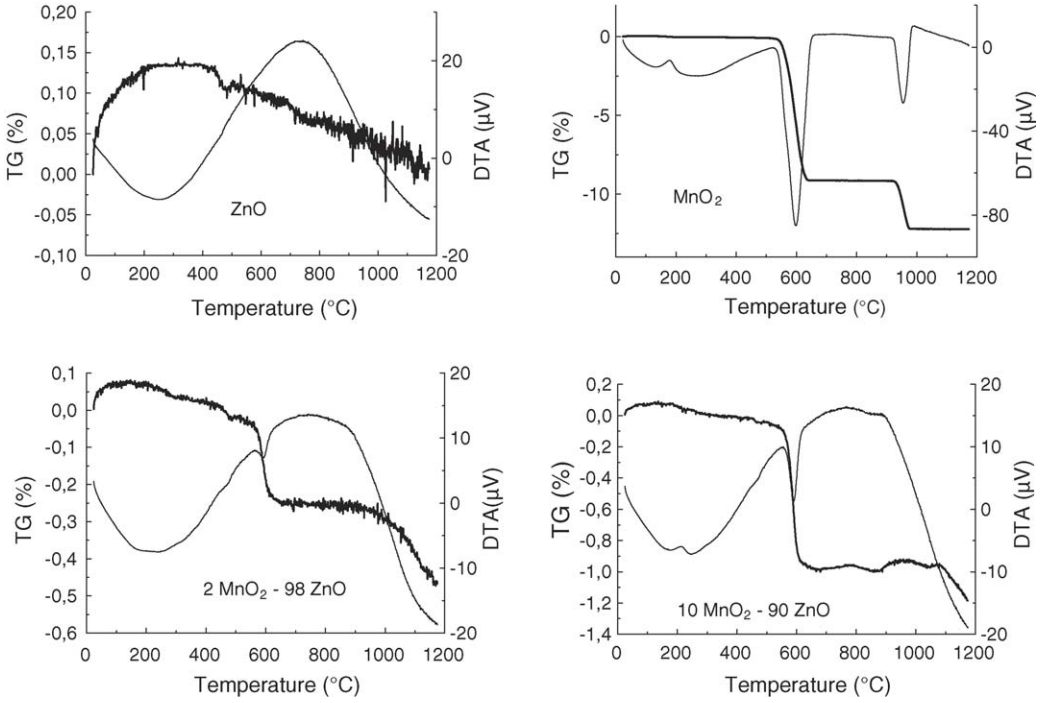

Fig. 1. DTA-TG data for ZnO (smaller particle) and MnO_2 raw materials and mixtures (bold lines correspond to TG curves).

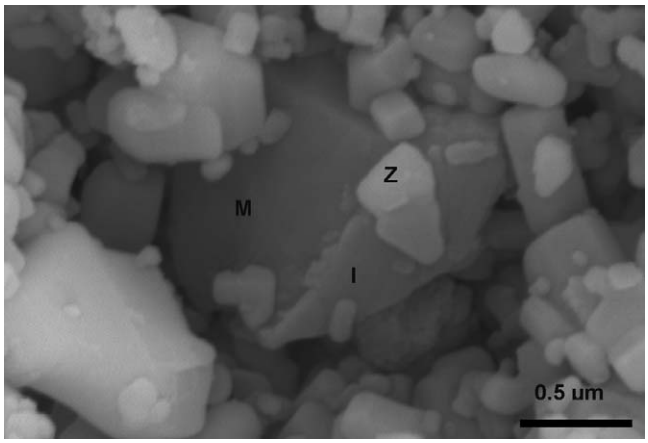

Fig. 2. FESEM micrograph of fresh fracture surface of sample $10MnO_2$–90ZnO 500 °C 12 h.

related to the reduction of Mn_2O_3 to Mn_3O_4 was not detected. This could be due to the difficulty of seeing the peak for such a low Mn content or that the associated mass losses required temperatures higher than 1000 °C. Hence, so this behaviour could indicate that the reaction with ZnO maintains the stable Mn^{3+} oxidation state.

In a previous contribution[7] we established a progressive reduction of the Mn^{4+} to Mn^{3+}, when the ZnO contribution was subtracted from that of the mixture between 200 and 600 °C. This reaction is related to the Zn^{2+} diffusion into the manganese particles. From XRD analysis the mixtures treated at 500 °C for 12 h showed[7] the coexistence of MnO_2, Mn_2O_3 and $Zn_xMn_{3-x}O_4$. The appearance of a ferromagnetic response at room temperature is consistent with the coexistence of Mn^{3+} and Mn^{4+} at the interface of the Zn diffusion front in manganese particles. However, the coexistence of different phases in the samples could reflect an inhomogeneous process and both the appearance of a new phase and the stability of the Mn^{3+} oxidation state suggests a reaction with ZnO.

FESEM observation of $10MnO_2$–90ZnO treated at 500 °C for 12 h (Fig. 2) revealed a microstructure that comprises small ZnO unreacted particles and bigger particles related to the manganese containing phases. The density of this sample is 3.19 g/cm^3, slightly higher than the expected for an unreacted mixture, 3.11 g/cm^3 but far away from the dense structure, 5.5 g/cm^3. The appearance of a second phase at the surface of the manganese particles is relevant, as it implies a limited reaction, but no true densification process. In all cases, EDX analysis confirmed the presence of zinc in the manganese particles. New phases appeared at the surface of the manganese particle. High-resolution electron microscopy, HREM, characterized such phases as spinel rich in Mn-rich spinel structure[7]. The Mn/Zn ratio of this spinel phase averages between 2.5 and 4 with changes inside each particle. As the temperature of the thermal treatment increased, the proportion of the spinel like phase increased and the ferromagnetic response decreased. In order to understand this phase formation, XRD of higher mixtures with higher Mn/Zn than the correspondent to $2MnO_2$–98ZnO and $10MnO_2$–90ZnO samples were studied.

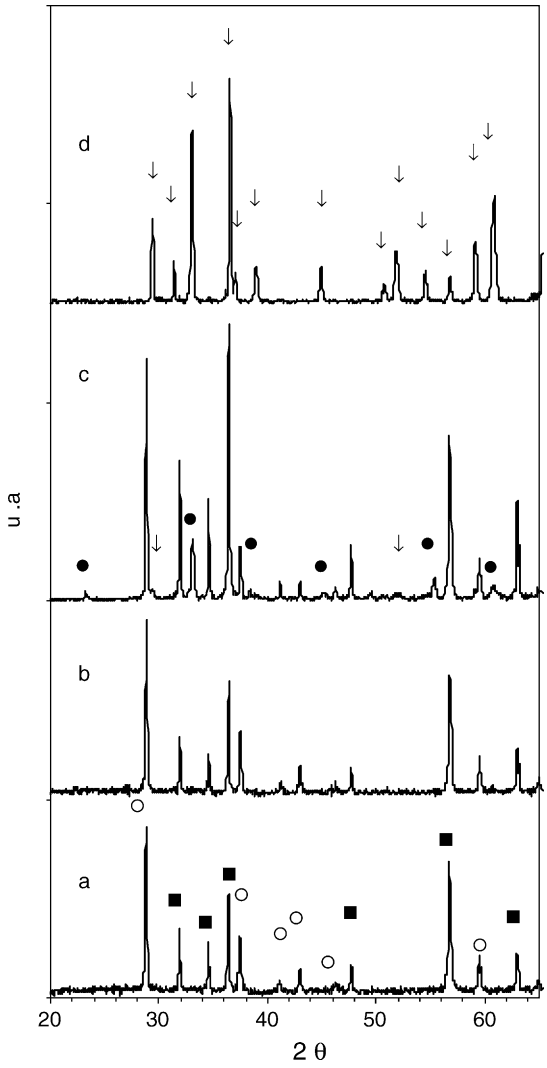

Fig. 3. XRD spectra of samples with Mn/Zn ratio 2:1 with different thermal treatments: (a) starting mixture, (b) pre-reacted 400 °C 8 h, (c) 500 °C 12 h, and (d) 900 °C 12 h (■ ZnO, ◯ MnO_2, ● Mn_2O_3, ↓ $ZnMn_2O_4$).

Figs. 3 and 4 show the XRD patterns of higher Mn/Zn ratio, thermally treated samples. XRD were recorded for the pellet surface because the grinding process introduces enough energy to complete the transformation of MnO_2 into Mn_2O_3.[6] This fact has induced to an erroneous interpretation in former studies.[4,11] A similar procedure carried out with pure MnO_2 did not show the same process and thus implies that the manganese metastability is conferred by the Zn reaction. Fig. 3a and b show the XRD patterns from the starting mixture and 400 °C for 8 h pre-reacted spinel base composition, Mn/Zn ratio of 2:1, respectively. In both cases, only the presence of the starting materials, ZnO and MnO_2, is observed, having the same intensity peaks. Accordingly, from the crystalline point of view, the powder pre-reaction step served as a homogenization step rather than a reaction procedure. The pellets thermally treated at 500 °C for 12 h (Fig. 3c) revealed in addition to the raw material the presence of Mn_2O_3 and spinel phase. The 900 °C for 12 h thermally treated material (Fig. 3d) clearly showed a single spinel phase, $ZnMn_2O_4$. Higher and lower Mn/Zn ratios than that for the spinel sam-

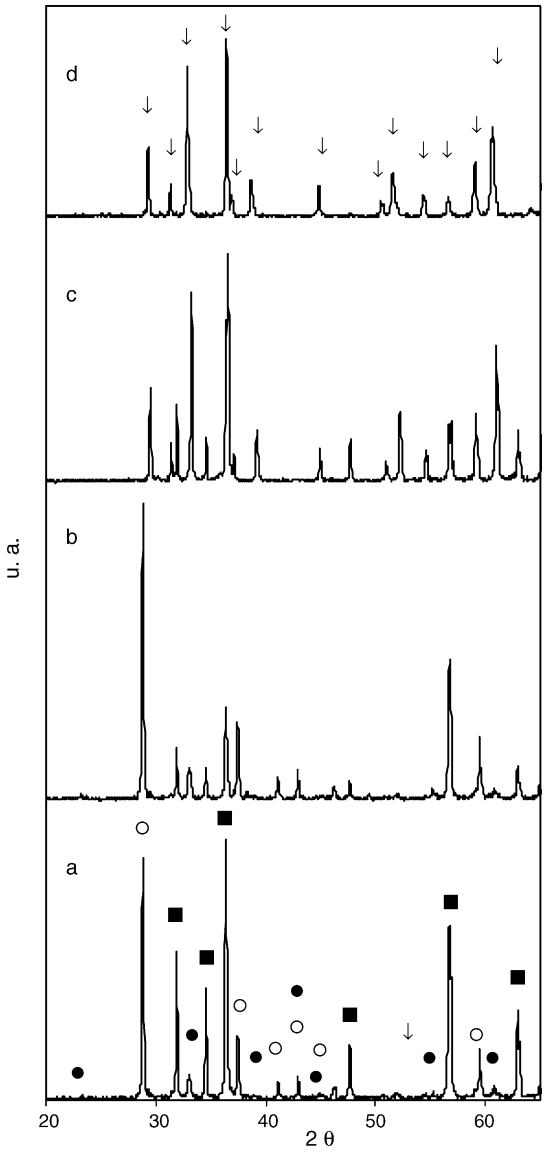

Fig. 4. XRD spectra of samples with different Mn/Zn ratios and different thermal treatments: (a) 1:1 at 500 °C 12 h, (b) 3:1 at 500 °C 12 h, (c) 1:1 at 900 °C 12 h, and (d) 3:1 at 900 °C 12 h (■ ZnO, ◯ MnO_2, ● Mn_2O_3, ↓ $ZnMn_2O_4$).

ples, thermally treated at 500 and 900 °C for 12 h, complete the information on the system reactivity (Fig. 4). At 500 °C, a larger concentration of starting MnO_2, leads to a larger fraction of unreacted MnO_2 in the treated sample. This is a sign that the appearance of both the Mn_2O_3 and the spinel phase are rather independent of the starting manganese content for a determined amount of manganese.

Annealing pellets with Mn/Zn ratio of 1:1 (Fig. 4c), less Mn than required to form the spinel, at 900 °C for 12 h, yield to the formation of the spinel plus unreacted ZnO. On the other hand, pellets with Mn/Zn ratio of 3:1 (Fig. 4d) only formed spinel type phase at that temperature. This spinel is a manganese rich phase that confirms the presence of Mn/Zn ratios ranging from 2.5 to 4 as previously reported.[7]

Fig. 5 summarizes the M_s values of the ferromagnetic response at room temperature for the different samples exposed

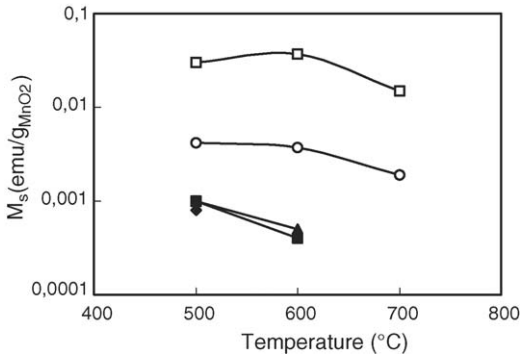

Fig. 5. Saturation magnetization values of the RT FM response for different compositions as a function of the thermal treatment temperature (□ $2MnO_2$–98ZnO, ◯ $10MnO_2$–90ZnO, ■ 1:1 Mn/Zn, ● 2:1 Mn/Zn, ▲ 3:1 Mn/Zn).

to different thermal treatments. The lower the amount of manganese in initial mixture, the larger the FM response. A larger Mn/Zn ratio gave the same FM RT response in agreement with the XRD results, being related to the same amount of Mn_2O_3 and spinel above discussed. The simultaneous increase in the amount of the spinel and the reduction of the magnetization implies that this phase is not the origin of the FM response. Samples with smaller ZnO particles as raw material show a 50% higher magnetization value at room temperature, only for the $2MnO_2$–98ZnO composition, 6×10^{-3} emu/g_{MnO_2}, whilst the rest of compositions show similar values. By reducing ZnO particle size the amount of RT FM phase was favoured, but only for the low manganese content samples.

Fig. 6 shows the Raman spectra of the spinel, manganese and ZnO reference samples, $10MnO_2$–90ZnO, and $2MnO_2$–98ZnO treated at 500 °C for 12 h samples. Raman modes for MnO_2 500 °C 12 h in the region of 200–800 cm^{-1} appear at 512, 645 and 739 cm^{-1}. In addition to modes corresponding to Mn^{4+}, a mode at 302 cm^{-1} denotes the slight presence of Mn_2O_3 in the sample that was not revealed by XRD. The Raman spectra for Mn_2O_3 shows modes at 302 and 690 cm^{-1}. Single crystalline spinel phase $ZnMn_2O_4$ shows Raman modes at 295, 321, 361, 380, 477 and 674 cm^{-1}. The modes at 295 and 674 cm^{-1} are related to the manganese cations while the other seem more related to the zinc cations. Raman modes of samples $2MnO_2$–98ZnO and $10MnO_2$–90ZnO 500 °C 12 h, show two overlapping peaks at 674 and 659 cm^{-1}, one of them is characteristic of the Mn cations in the spinel phase and the other is related to an intermediate oxidation state.[19] Other peaks could be also attributed to this intermediate oxidation state as the peak at 534 cm^{-1}. The Raman modes for ZnO peaks in this range are 325, 375 and 436 cm^{-1}, the last one is the most intense. It is worthy to note that the RT FM was found only in samples that show this intermediate oxidation state where Mn^{3+} and Mn^{4+} coexist and the double-exchange mechanism allows the system to exhibit a large Curie temperature.[20,21]

Fig. 7 shows the Raman spectra for the samples with larger manganese content. All samples treated at 500 °C showed the ZnO peak of 436 cm^{-1} that indicates the presence of unreacted powder. In addition to the intermediate oxidation state peak and that for the spinel, peaks corresponding to the Mn_5O_8 phase were

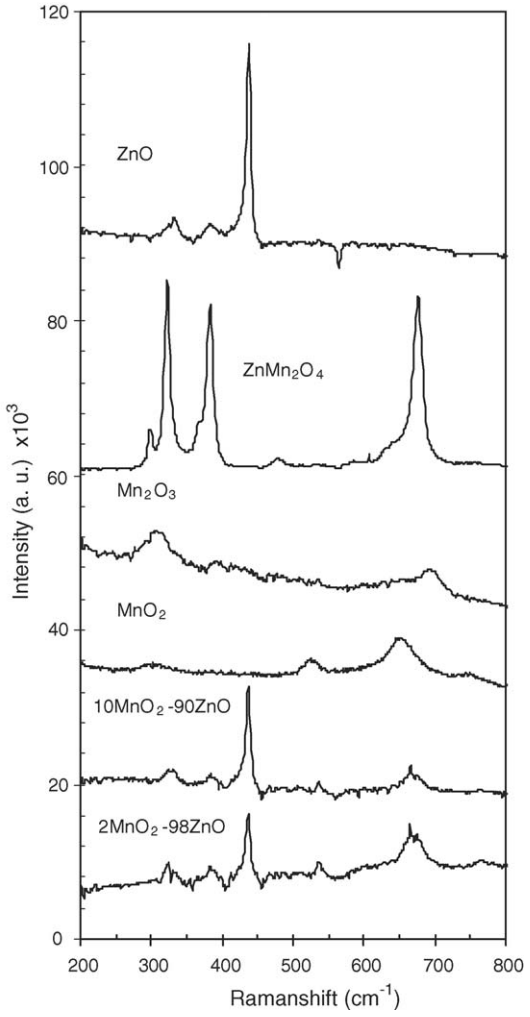

Fig. 6. Raman spectra for $2MnO_2$–98ZnO 500 °C 12h, $10MnO_2$–90ZnO 500 °C 12 h, MnO_2, Mn_2O_3, $ZnMn_2O_4$ and ZnO samples.

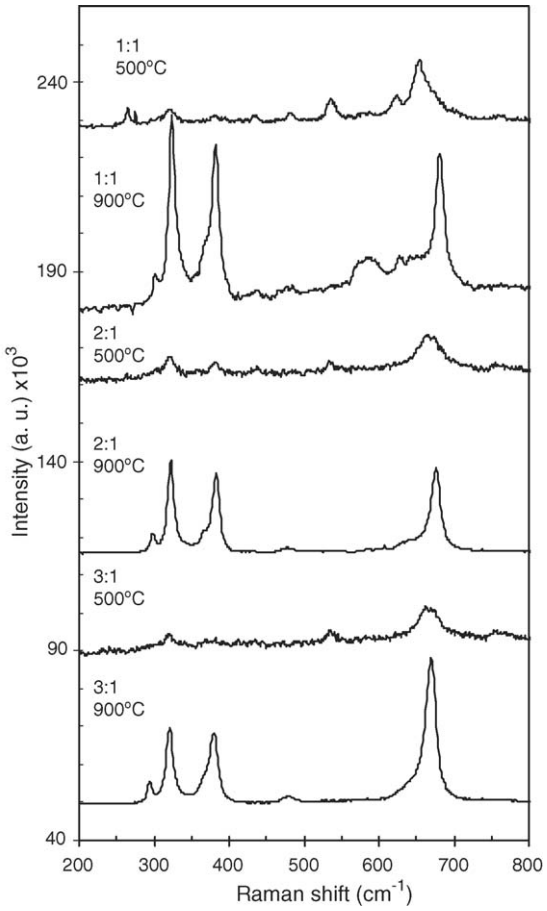

Fig. 7. Raman spectra for samples with different Mn/Zn ratios, thermally treated.

clearly found in the 1:1 Mn/Zn ratio samples. The 900 °C 12 h samples show spinel as the main phase. Samples with Mn/Zn ratios of 2:1 and 3:1 show the same spectra according to the XRD spectra, indicating the same structure and the capability of the spinel to incorporate more manganese cations. The structural similarities between Mn_2O_3 and the spinel could be the reason for such behaviour. The sample with Mn/Zn ratio of 1:1 shows the presence of unreacted ZnO and an unassigned peak at 583 cm^{-1}.

Moreover, in order to verify the chemical state and surface concentration of manganese ions in the samples they were analyzed by XPS. The Mn 2p core-level spectra of samples in the system Zn–Mn–O shown in Fig. 8a and the corresponding binding energies are presented in Table 1. For comparison purpose, the Mn 2p profiles of MnO_2, Mn_2O_3 and MnO reference samples are displayed in Fig. 8b. Confirmation of the reduction of Mn^{4+} into Mn^{3+} was provided by XPS. The binding energies (BE) of the principal Mn $2p_{3/2}$ peak for all the samples fall within 641.6–641.8 eV range. In comparison with the reference spectra (Fig. 8b) and also with many literature reports[22–24] these BEs values are typical of Mn^{3+}-containing oxides such as Mn_3O_4 and Mn_2O_3, whereas the Mn^{4+}-containing materials are reported to have BEs values between 642.0 and 642.6 eV.[22,24] Thus, all the Mn atoms located at the surface are reduced to the 3+ oxidation state because of the Zn diffusion. Although the system is not homogeneous, the structural analysis confirms the absence of Mn^{4+} at the pellet surface. Since Mn^{4+} has been detected by XRD, this means that an interface containing Mn^{4+} and Mn^{3+} exists. This result supports the proposed model of a Zn diffusion front inside the manganese grain as the origin of the interface double-exchange ferromagnetism in the Mn–Zn–O system.[7] This interface would disappear when the MnO_2 does.

Surface Mn/Zn ratios have been calculated from the intensity ratios normalized by atomic sensitivity factors[25] and are also

Table 1
Binding energies (eV) and surface atomic ratios of samples

Sample	Mn $2p_{3/2}$	Zn $2p_{3/2}$	Mn/Zn at
MnO	641.6	–	–
Mn_2O_3	641.8	–	–
MnO_2	642.6	–	–
ZnO	–	1021.8	–
3:1 Mn/Zn	641.8	1021.7	2.10
2:1 Mn/Zn	641.6	1021.7	1.21
1:1 Mn/Zn	641.7	1021.8	0.89
10% MnO_2–90% ZnO	641.6	1021.7	0.094
2% MnO_2–98% ZnO	641.7	1021.8	0.019

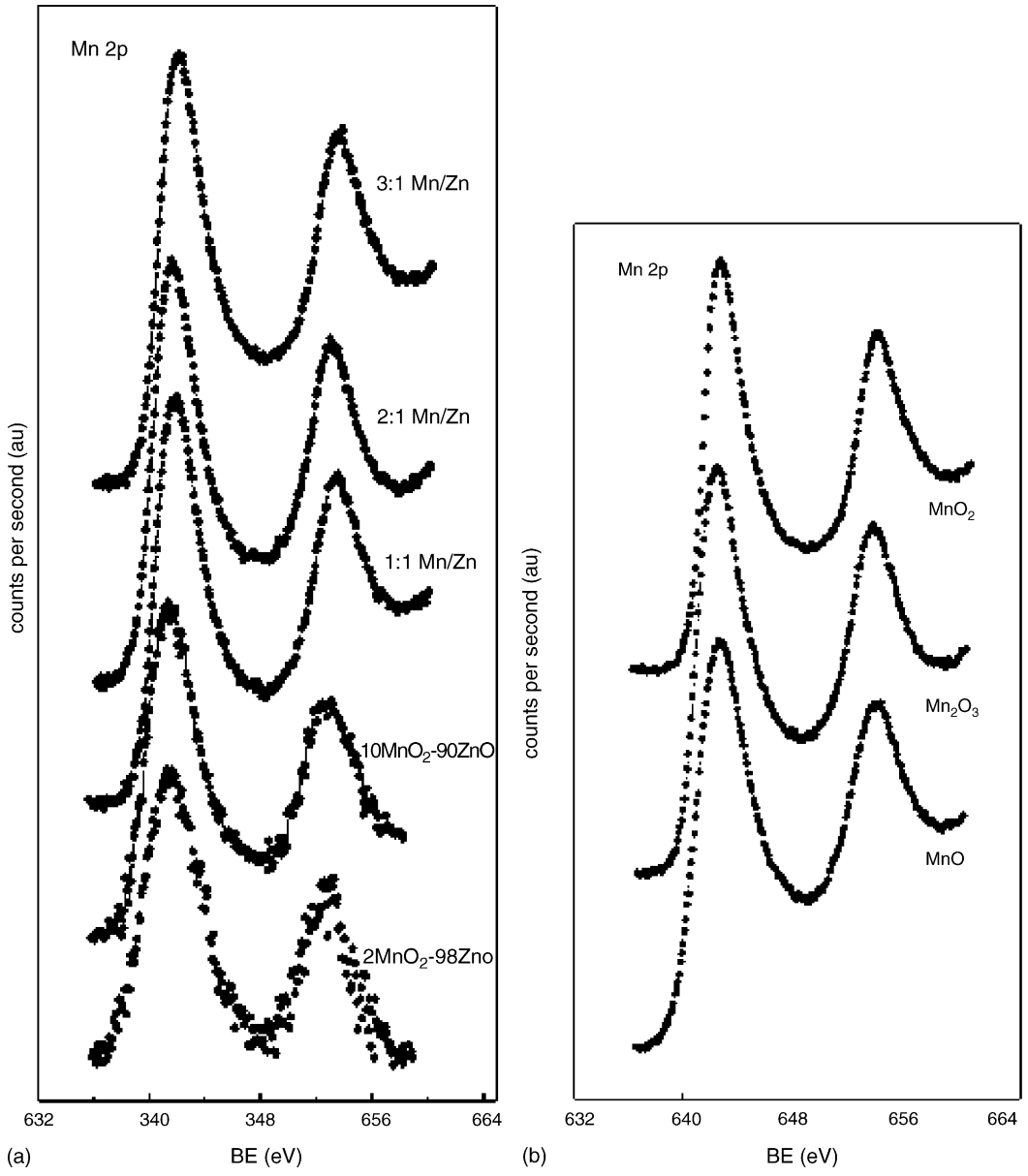

Fig. 8. Mn 2p core-level spectra for samples thermally treated at 500 °C: (a) $2MnO_2$–98ZnO (magnified ×18), $10MnO_2$–90ZnO (magnified ×6), 1:1 Mn/Zn, 2:1 Mn/Zn, 3:1 Mn/Zn and (b) reference samples MnO_2, Mn_2O_3 and MnO.

summarized in Table 1 (last column). In order to see if Zn and Mn are homogeneously distributed, experimental Mn/Zn atomic ratios are plotted against the nominal Mn/Zn ratios in Fig. 9. As can be seen, the experimental Mn/Zn ratios almost coincide with the nominal ones in the $0 < x \leq 1$ composition region; however, some deviation from linearity happens for Mn/Zn ratios of 2 and 3. This latter finding suggests that formation of a Zn-free Mn^{3+}-containing phase coexist with the $ZnMn_2O_4$ spinel phase. Thus, the appearance of Zn-free manganese oxide species in the region of high Mn-contents would be related to the decay of M_s detected for these samples as then there is no coexistence of Mn^{4+} and Mn^{3+} at the diffusion front.

PLD thin films preserve the composition of the target, but the oxygen content could be changed by the partial pressure in the reaction chamber. Thin films of $10MnO_2$–90ZnO grown at 600 °C at a $p(O_2)$ of 2×10^{-2} mbar exhibit a saturation magnetization of 1.3 emu cm^{-3} (Fig. 10a) that is similar to the best value reported for thin films.[7] The presence of excess oxygen during PLD growth prevents the reduction of manganese and thus the interface state is maintained. Nevertheless, taking into account the preliminary results for pellets it is difficult to understand why this sample, $10MnO_2$–90ZnO, does not show any manganese-related peaks in the XRD pattern (Fig. 10b). The reason could be due to the fact that when growing a pure MnO_2 thin film directly over the substrate an amorphous pattern is observed. Nevertheless, when growing a pure MnO_2 thin film over a *c*-axis oriented ZnO (1 1 1) films some manganese oxide peaks can be observed. Previous reports correlated the absence of manganese peaks in thin films to the solid solution of Mn^{2+} into the ZnO matrix and thus attributed the FM origin to the Zener model.[4,11] The pres-

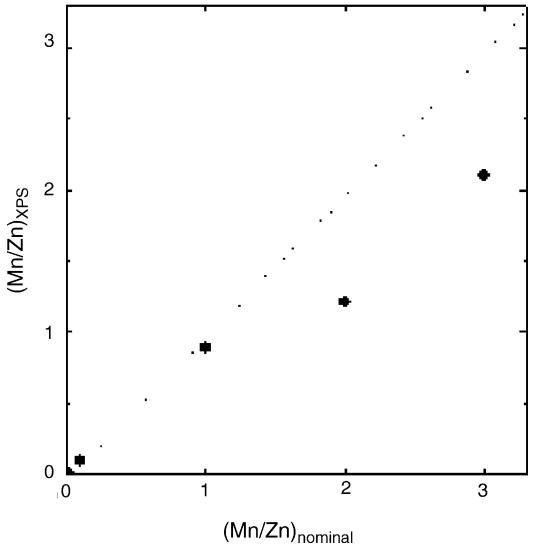

Fig. 9. Comparison of Mn/Zn surface atomic ratios derived from XPS with the nominal ones.

ence of higher oxidation state in thermally treated samples at higher temperatures, Mn^{3+}, denotes different possible process as the crystallization of Mn_2O_3 from the amorphous MnO_2 or the spinel, destroys the RT FM response. The possible formation of manganese oxide clusters at higher temperatures reported by Sharma el al.[11] is thus explained.

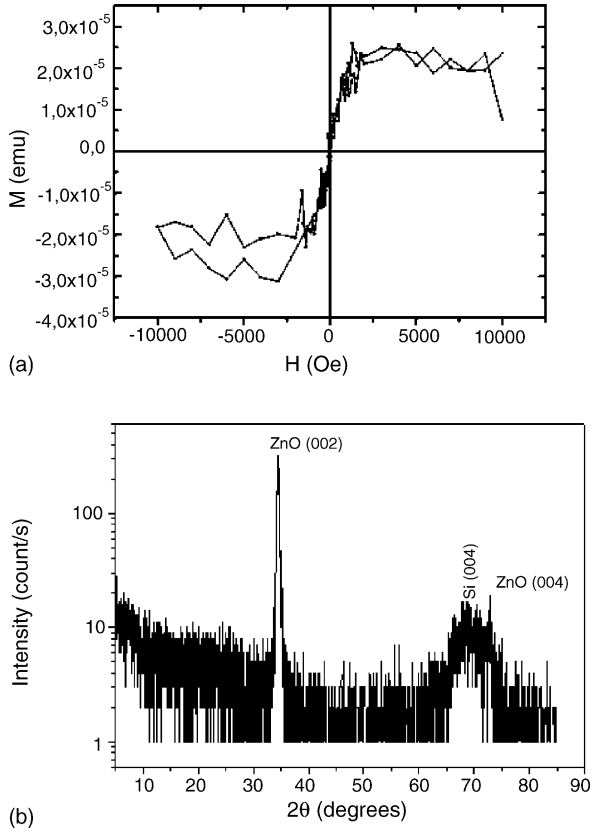

Fig. 10. $10MnO_2$–$90ZnO$ thin film grown at 600 °C and $p(O_2)$ 2×10^{-2} mbars. (a) Hysteresis loop and (b) XRD diffraction pattern.

4. Conclusions

With the results reported in this contribution the reactivity of MnO_2 in presence of ZnO is clarified. At low temperatures (500 °C) there is a limited reaction without densification. Mn cations do not incorporate into the ZnO lattice substitutionally, but it is the Zn that diffuses into the manganese oxide grains, acting as a retardant of the $MnO_2 \rightarrow Mn_2O_3$ reduction.

The ferromagnetic phase is related to the simultaneous presence of Mn^{+3} and Mn^{+4} ions at the Zn diffusion front into the manganese oxide grains. The presence of Mn^{3+} cations in the MnO_2 does not imply the appearance of FM response, and therefore, the double exchange mechanism required the presence of Zn cations. The lower the amount of manganese in the mixture, the larger the ferromagnetic response.

The spinel phase is the stable one at higher temperatures. This spinel phase allows the incorporation of excess Mn. As the spinel phase progress, the reduction of the M_s implies that the origin of the FM response is not associated with the metastable phase.

The reaction mechanism explains the origin of the room temperature ferromagnetism recently discovered in the Zn–Mn–O system as a base material for spintronic applications.

Acknowledgments

This work has been financially supported by CICYT MAT2004-04843-C02-01 and the University Complutense through the project PR1/05-13325.

References

1. Ohno, H., Making nonmagnetic semiconductors ferromagnetic. *Science*, 1998, **281**, 951–956.
2. Tanaka, M., Spintronic: recent progress and tomorrow's challenges. *J. Cryst. Growth.*, 2005, **278**, 25–37.
3. Dietl, T., Ohno, H., Matsukura, F., Cibert, J. and Ferrand, D., Zener model description of ferromagnetism in zinc-blende magnetic semiconductors. *Science*, 2003, **287**, 1019–1022.
4. Sharma, P., Gupta, A., Rao, K. V., Owens, F. J., Sharma, R., Ahuja, R. *et al.*, Ferromagnetism above room temperature in bulk and transparent thin films of Mn-doped ZnO. *Nat. Mater.*, 2003, **2**(10), 673–677.
5. Kundaliya, D., Ogale, S. B., Lofland, S. E., Dhar, S., Meeting, C. J., Shinde, S. R. *et al.*, On the origin of high-temperature ferromagnetism in the low-temperature processed Mn–Zn–O system. *Nat. Mater.*, 2004, **3**(10), 709–714.
6. Costa-Krämer, J. L., Briones, F., Fernandez, J. F., Caballero, A. C., Villegas, M., Diaz, M. *et al.*, Nanostructure and magnetic properties of MnZnO system, a room temperature magnetic semiconductor? *Nanotechnology*, 2005, **16**, 214–218.
7. García, M. A., Ruiz-Gonzalez, M. L., Quesada, A., Costa-Krämer, J. L., Fernández, J. F., Khatib, S. J. *et al.*, Interface double-exchange ferromagnetism in the Mn–Zn–O system: new class of biphase magnetism. *Phys. Rev. Lett.*, 2005, **94**, 217206.
8. Huang, X., Makmal, A., Chelikowsky, J. R. and Kronik, L., Size-dependent spintronic properties of dilute magnetic semiconductor nanocrystals. *Phys. Rev. Lett.*, 2005, **94**, 236801.
9. Venkatesan, Fitzgerald, C. B., Lunney, J. G. and Coey, J. M. D., Anisotropic ferromagnetism in substituted zinc oxide. *Phys. Rev. Lett.*, 2004, **93**, 177206.
10. Sluiter, M. H. F., Kawazoe, Y., Sharma, P., Inoue, A., Raju, A. R. and Waghmare, U. V., First principles based design and experimental evidence

for ZnO-based ferromagnet at room temperature. *Phys. Rev. Lett.*, 2005, **94**, 187204.
11. Sharma, P., Gupta, A., Owens, F. J., Inoue, A. and Rao, K. V., Room temperature spintronic material-Mn doped revisited. *J. Magn. Magn. Mater.*, 2004, **282**, 115–121.
12. Rao, C. N. R. and Deepak, F. L., Absence of ferromagnetism in Mn- and Co-doped ZnO. *J. Mater. Chem.*, 2005, **15**(5), 573–578.
13. Kittilstved, K. R., Norberg, N. S. and Gamelin, D. R., Chemical manipulation of high-T_C ferromagnetism in ZnO diluted magnetic semiconductors. *Phys. Rev. Lett.*, 2005, **94**, 147209.
14. Peiteado, M., Zinc oxide based varistors. *Bol. Soc. Esp. Ceram. V.*, 2005, **44**(2), 77–88.
15. Fernandez-Hevia, D., Caballero, A. C., Frutos, J. and Fernandez, J. F., Application of broadband admitance Spectroscopy to microstructure control of the electrical properties of ceramic varistors. *Bol. Soc. Esp. Ceram. V.*, 2004, **43**(3), 674–678.
16. Fernandez-Hevia, D., Peiteado, M., de Frutos, J., Caballero, A. C. and Fernandez, J. F., Wide range dielectric spectroscopy of ZnO-based varistors as a function of sintering time. *J. Eur. Ceram. Soc.*, 2004, **24**, 1205–1208.
17. Caballero, A. C., Fernandez, J. F., Moure, C., Duran, P. and Chiang, Y. M., Grain growth control and dopant distribution in ZnO-doped $BaTiO_3$. *J. Am. Ceram. Soc.*, 1998, **81**, 4939–4944.
18. Stobbe, E. R., de Boer, B. A. and Geuss, J. W., The reduction and oxidation behaviour of manganese oxides. *Catal. Today*, 1999, **47**, 161–167.
19. Zaki, M. I., Hasan, M. A., Pasupulety, L. and Kurami, K., Thermochemistry of manganese oxides in reactive gas atmospheres: probing redox compositions in the decomposition course $MnO_2 \rightarrow MnO$. *Thermochim. Acta*, 1997, **303**, 171–181.
20. Salamon, M. B. and Jaime, M., The physics of manganites: structure and transport. *Rev. Mod. Phys.*, 2001, **73**, 583–628.
21. Alonso, J., Gonzalez-Calbet, J. M., Vallet-Regi, J. M., Martinez, J. L., Rojo, J. M. and Hernando, A., Role of calcium ions as doped-hole attractors in destabilizing charge-ordered states in Mn perovskites. *Phys. Rev. B*, 2001, **64**, 172410.
22. Gautier, L., Rios, E., Gracia, M., Marco, J. F. and Gancedo, J. R., Characterisation by X-ray photoelectron Spectroscopy of thin $Mn_xCo_{3-x}O_4$ $(1 \geq x \geq 0)$ spinel films prepared by low temperature spray pyrolisis. *Thin Solid Films*, 1997, **311**(1/2), 51–57.
23. Wagner, C. D., Riggs, W. M., Davis, L. E., Moulder, J. F. and Muilenberg, G. E., In *Handbook of X-Ray Photoelectron Spectroscopy*. Physical Electronics Industries, Eden Prairie, MN, 1979, p. 188.
24. Nesbitt, H. W. and Banerjee, D., Interpretation of XPS Mn(2p) spectra of Mn oxyhydroxides and constraints of the mechanisms of MnO_2 precipitation. *Am. Mineral.*, 1998, **83**(3/4), 305–315.
25. Wagner, C. D., Davis, L. E., Zeller, M. V., Taylor, J. A., Raymond, R. H. and Gale, L. H., Empirical atomic sensitivity factors for quantitative analysis by electron spectroscopy for chemical analysis. *Surf. Interf. Anal.*, 1981, **3**(5), 211–225.